Stratigraphy of the 8.5 – 9.0 ka B.P. Citlaltépetl pumice fallout sequence

Andrea Rossotti[1,*], Gerardo Carrasco-Núñez[2]

[1] Posgrado en Ciencias de la Tierra
[2] Centro de Geociencias
Universidad Nacional Autónoma de México, Campus Juriquilla, A.P. 1–742,
76001 Querétaro, Qro., Mexico.
* andrea.rossotti@geociencias.unam.mx

ABSTRACT

Citlaltépetl is an active volcano presently in a dormant state, belonging to the easternmost part of the Mexican Volcanic Belt. Although the volcano is characterized by long periods of volcanic repose, some explosive plinian eruptions occurred in Holocene time. In particular, an eruptive period between 8.5–9.0 ka B.P. originated an alternated sequence of pumice and scoria flows called Citlaltépetl Ignimbrite (0.26 km³ DRE) and a few ash and lapilli fallout deposits (Citlaltépetl Pumice) with a wide dispersion range around the cone. In this work we present a detailed reconstruction of the fallout Citlaltépetl Pumice stratigraphy based on the combined study of 107 vertical sections, grain-size and component analysis of each layer. The eruptive sequence comprises a succession of pyroclastic deposits, including four major eruptive episodes.

New radiocarbon dating on charcoal fragments interbedded in the flow deposits beneath the fallout and in the fallout itself show ages younger than 9,475±160 yr. B.P. and older than 8,505±50 yr. B.P., respectively, which is in accordance with previous dates. Stratigraphy and dating allowed a precise stratigraphic correlation of the most representative fallout deposits of the Holocene history of Citlaltépetl volcano and their relationship with associated pyroclastic flows. Such data provide new insights on the formation and eruptive history of the Citlaltépetl Ignimbrite that is of basic importance for further eruptive column modeling with important implications in the volcanic hazard assessment.

Key words: Citlaltépetl volcano, fallout deposit, granulometry, volcanic stratigraphy, correlation, radiocarbon dating.

RESUMEN

Citlaltépetl es un volcán activo, actualmente en estado de reposo, que pertenece a la parte más oriental del Cinturón Volcánico Mexicano. Aunque el volcán se caracteriza por periodos prolongados de reposo, durante el Holoceno ocurrieron algunas explosivas de tipo pliniano. En particular, durante el periodo eruptivo entre 8.5–9.0 ka B.P. se originó una secuencia alternada consistente en depósitos de flujo de pómez y escoria denominados Ignimbrita Citlaltépetl (0.26 km³ DRE) y en depósitos de caída de ceniza y lapilli (Pómez Citlaltépetl) que tienen una amplia dispersión en las laderas del Citlaltépetl. En este trabajo presentamos una reconstrucción detallada de la estratigrafía de la Pómez Citlaltépetl basada en el estudio combinado de 107 secciones estratigráficas verticales y en el análisis de componentes y granulometría de cada capa. La secuencia está constituida por una sucesión de capas piroclásticas, cuatro de las cuales corresponden a episodios eruptivos más importantes. Los nuevos fechamientos de radiocarbono en los depósitos de flujo subyacentes a las caídas y en los mismos depósitos de caída, proporcionan una edad más joven que 9,475±160 años B.P. y más vieja que 8,505±50 años B.P., respectivamente, lo cual es congruente con los fechamientos reportados en trabajos previos. La

estratigrafía y los fechamientos realizados permitieron hacer una correlación estratigráfica precisa de los depósitos de caída más importantes de la historia de inicio del Holoceno del Citlaltépetl y su relación con los flujos piroclásticos asociados. Estos datos proporcionan una visión más detallada sobre la historia eruptiva de la Ignimbrita Citlaltépetl que servirá como base para elaborar un modelo futuro de columna eruptiva con implicaciones importantes en la evaluación del peligro volcánico.

Palabras clave: Volcán Citlaltépetl, depósito de caída, granulometría, estratigrafía volcánica, correlación, fechamiento de radiocarbono.

INTRODUCTION

Citlaltépetl ("Mountain of the star") or Pico de Orizaba is an andesitic stratovolcano presently in a dormant state. With its 5,685 m a.s.l., it is the highest peak in Mexico and the highest volcano in North America. It rises in the easternmost part of the Mexican Volcanic Belt between the States of Puebla and Veracruz (W 97°16' and N 19°02') (Figure 1). The complex structure of Citlaltépetl, built entirely during the Quaternary age, covers the Mesozoic carbonate platform country rock with more than 800 km³ (Carrasco-Núñez, 1997) of volcanic products and seals out a NW–SE normal faulting system that lowered by 1,300 m the eastern side of Mexico with respect to the inner highlands (Carrasco-Núñez, 1993). As part of the most important explosive eruptive epoch (following the terminology proposed by Fisher and Schmincke, 1984) of the Holocene history of the volcano, a thick sequence of widely distributed fallout deposits was produced, which is named here "Citlaltépetl Pumice" (CP). This deposit has a wide distribution around the volcano and crops out mainly on the topographic heights of the Citlaltépetl slopes. This sequence is interbedded with high density pyroclastic flows formed between 8.5 and 9.0 ka B.P., which are defined as the Citlaltépetl Ignimbrite (CI) (Carrasco-Núñez and Rose, 1995). CI consists of two sets of composite pyroclastic flows (lower and upper) separated by distinctive pyroclastic fallout deposits.

In addition to the study of the Citlaltépetl Ignimbrite by Carrasco-Núñez and Rose (1995), Höskuldsson (1993) and Höskuldsson and Robin (1993) provide a general description of different eruptive events in the late Pleistocene–Holocene. This paper focuses on the study of the complete stratigraphy of the CP as well as its vertical and lateral stratigraphic relationships with the associated high density pyroclastic flows based on a new set of stratigraphic columns, grain-size, component analysis, radiocarbon age correlation and mineralogical analysis. Since this paper is focused only on the stratigraphy and correlation of the Citlaltépetl Pumice deposits, it will serve as a basic study for a complete understanding of the eruption dynamics, which is out of the scope of this study and will

be published elsewhere.

Although the historic activity of Citlaltépetl has been predominantly effusive with only minor ash eruptions and/or fumarolic activity (Crausaz, 1994), repeated plinian or sub-plinian activity has also occurred during the Holocene and could occur in the future. This work is an effort toward the understanding of the eruptive conditions that triggered the high explosive epoch which can be used for hazard assessment purposes.

SUMMARY OF THE GEOLOGICAL EVOLUTION OF CITLALTÉPETL VOLCANO

The first description of the geology of Citlaltépetl volcano and Holocene pyroclastic deposits was made by Robin and Cantagrel (1982) however, at the light of the most recent studies (Carrasco-Núñez 2000) the evolution of the Citlaltépetl volcano can be divided into the following three main stages:

Torrecillas stage

At this stage took place the formation of a large, mostly effusive andesite cone (650–300 ka B.P.), overlying the Cretaceous carbonate bedrock. The oldest lavas are olivine-bearing basalts that change to porphyritic plagioclase-bearing andesites and dacites in the middle and upper part of the sequence. Partial sector collapse of the Torrecillas cone occurred between 290 and 210 ka B.P. producing the ~20 km³ "Jamapa" debris avalanche which traveled up to 75 km downstream.

Espolón de Oro stage

This stage involves the growth of a dacitic second cone of at about 210 ka B.P. above the Torrecillas remnants. It started with the eruption of amphibole-bearing dacites, followed by porphyritic andesites and basaltic andesites. Cone collapse occurred at about 16.5 ka B.P. (Sheridan,
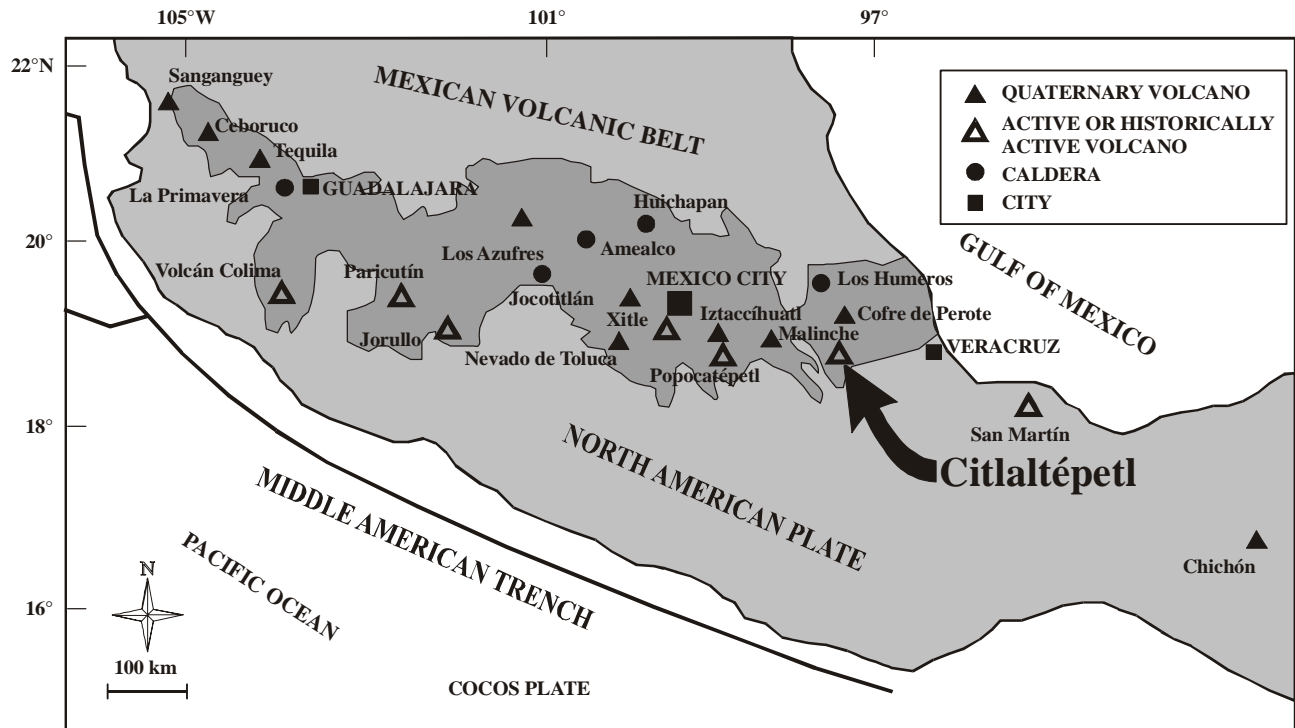
Figure 1. Location of Citlaltépetl and other volcanoes within the Mexican Volcanic Belt.

unpublished data) producing the ~2 km³ Teteltzingo debris avalanche-induced lahar (Carrasco-Núñez *et al.*, 1993).

Citlaltépetl stage

Construction of the present Citlaltépetl cone was characterized by the emplacement of viscous dacitic lavas, interrupted by numerous explosive eruptions, which include pyroclastic-flow forming eruptions at 13 ka B.P. and the 8.5–9.0 ka B.P. Citlaltépetl Ignimbrite and the Citlaltépetl Pumice studied in this paper. Block and ash flow forming eruptions occurred about 4 ka B.P. (Siebe *et al.*, 1993; Carrasco-Núñez and Rose, 1995). Some dacitic levee-sided lavas were emplaced in historic times (Carrasco-Núñez, 1997).

METHODOLOGY

Over 100 stratigraphic sections were measured, described and sampled. Locations of sampling log sites are listed in Table 1 and shown in Figure 2; for simplicity we used only the last two digits of the sampling site reference.

Samples from the best preserved 76 sites were dry-sieved and weighed in a range from -6 Φ (64 mm) to 10 Φ (0.98 μm) using mechanic sieves and two decimal digits scale for fractions from -6Φ to 4Φ (62.5 μm) and a photo-sedimentographer FRITSCH Analyst 20 for fine fractions from 5Φ to 10Φ in order to analyze the granulometry. Component analysis was carried out on -5Φ to -1Φ (2 mm) class range, using a binocular microscope for the finer particles. Grain size parameters (Inman, 1952), sorting index and frequency histograms were obtained with an adapted version of the Sequential Fragmentation/Transport (SFT) application, originally published by Wohletz (1983). Bulk density was measured in the field for each layer by tapping a sample of undisturbed primary tephra deposit into a PVC container of known volume and then measuring its weight and volume in accordance with Rodríguez *et al.* (2002).

The results for each layer are compared in Table 2. For crystal modal analysis and vesicularity measurements, 23 standard thin sections of both pumice and lithic clasts were analyzed from the representative layers. For each thin section, an area of about 66 mm² was selected and divided with a 500-knot lattice to form sub-areas of 0.33 by 0.40 mm (132 μm²) that were manually scanned under a binocular microscope. The minerals, glass or vesicles found in each knot were recorded with a proper point counter, and the relative volume percent and vesicularity were finally calculated (Table 3).

To facilitate descriptions, we introduce an empirical "Compaction Degree Scale" proposed in this paper (Table 4), which was used during fieldwork with the aim of easily quantify the degree of compaction of each single pyroclastic layer, and to allow the comparison of values obtained in

Table 1. Geographic coordinates (in UTM) and location of the 107 sites shown in Figure 2 ordered by azimuth and distance from vent.

Quadrant	Vent dist. (km)	Section	Site	Long	Lat	Altitude (m a.s.l.)	Locality
					(14 Q UTM)		
N	4.6	C-02-	91	681,584	2,109,499	4,005	N Hut
	5.1	C-02-	92	680,805	2,109,654	3,980	N Pico
	5.5	C-02-	93	680,199	2,109,689	3,937	N Pico
	5.8	C-02-	73	683,136	2,110,761	3,900	Nueva Vaquería W
	6.4	C-02-	98	681,371	2,110,803	3,734	N Pico
	6.5	C-02-	99	681,986	2,111,178	3,809	N Pico
	6.8	C-02-	74b	684,653	2,111,210	3,435	Pico NE
	7.0	C-02-	100	679,386	2,110,951	3,715	N Pico
	7.2	C-02-	97	679,111	2,110,960	3,668	N Pico
NE	8.0	C-02-	72	686,308	2,111,707	3,279	Nueva Vaquería W
	8.2	C-02-	85	685,972	2,112,436	3,262	W Nueva Vaquería
	8.6	C-02-	86	686,044	2,112,958	3,169	W Nueva Vaquería
	9.1	C-02-	55	686,054	2,113,103	3,130	El Jacal
	9.2	C-02-	51	688,203	2,111,888	3,058	Nueva Vaquería
	10.0	C-02-	84	688,266	2,112,886	2,941	N Nuova Vaquería
	11.1	C-02-	54	688,764	2,114,188	2,800	Tlacotiopa
	12.0	C-02-	52	689,777	2,114,260	2,680	Palo Gacho
	13.3	C-02-	53	691,345	2,114,909	2,550	Dos Caminos
	13.6	C-02-	83	691,389	2,114,710	2,544	Dos Caminos
	13.6	C-02-	49	694,464	2,111,041	2,350	Malacatepec
	14.1	C-02-	71	692,273	2,114,694	2,411	Tlcotiopa
	15.4	C-02-	43	695,968	2,111,766	2,450	S Ayahualulco
	15.5	C-02-	70	693,481	2,115,550	2,227	Tecoanapa
	16.4	C-02-	46	696,391	2,113,143	2,310	Ayahualulco
	16.5	C-02-	50	694,366	2,116,102	2,140	Excola
	16.6	C-02-	50b	694,419	2,116,146	2,149	Excola
	16.8	C-02-	44	697,098	2,112,838	2,250	Ayahualulco E
	17.2	C-02-	5	695,073	2,116,319	2,150	Excola
	17.4	C-02-	69	697,621	2,112,761	2,190	Ayahualulco E
	17.9	C-02-	57	693,304	2,118,828	2,080	NW Excola
	18.1	C-02-	42	698,201	2,113,010	2,040	Ayahualulco E
	19.0	C-02-	41	698,981	2,113,453	1,860	Ayahualulco E
E	6.8	C-02-	32	689,086	2,105,062	3,133	La Paloma
	8.2	C-02-	31	690,268	2,103,874	2,880	La Mata
	8.8	C-02-	76	690,993	2,105,743	3,061	Cuyachapa SW
	9.7	C-02-	28	691,670	2,102,107	2,524	Naranjillos W
	9.8	C-02-	30	691,805	2,102,565	2,600	Naranjillos N
	10.0	C-02-	75	692,304	2,104,837	2,874	Cuyachapa W
	10.5	C-02-	29	692,075	2,101,779	2,549	Naranjillos
	11.2	C-02-	35	693,442	2,106,424	2,570	Cuiyachapa E
	12.0	C-02-	34	693,900	2,108,169	2,490	El Potrerillo
	12.2	C-02-	36	694,475	2,105,950	2,519	Teteltzingo S
	12.3	C-02-	37	694,536	2,103,953	2,280	Tenixtepec
	12.5	C-02-	66	694,297	2,108,319	2,440	Teteltzingo-Cuyachap
	12.8	C-02-	67	694,887	2,107,919	2,395	Teteltzingo-Cuyachap
	13.8	C-02-	6	695,619	2,108,064	2,390	Teteltzingo
	16.2	C-02-	48	697,308	2,110,618	2,140	Ayahualulco S
	16.9	C-02-	47	697,868	2,111,458	2,100	Ayahualulco S
	22.8	C-02-	39	704,352	2,100,656	1,530	Tetla
	24.8	C-02-	40	706,946	2,102,743	1,370	Chocaman

Table 1. Continued.

Quadrant	Vent dist. (km)	Section	Site	Long	Lat (14 Q UTM)	Altitude (m a.s.l.)	Locality
SE	4.8	C-02-	4	686,664	2,102,381	3,610	Rancho Nuevo W
	5.6	C-02-	9	686,203	2,102,024	3,410	Rancho Nuevo W
	6.0	C-02-	88	687,297	2,100,857	3,234	Chinela
	6.5	C-02-	89	687,689	2,101,777	3,364	SE Pico
	6.5	C-02-	8	686,317	2,099,453	3,251	Pilancón SE
	6.8	C-02-	7	686,842	2,099,723	3,228	Pilancón
	7.9	C-02-	3	688,086	2,099,391	2,997	Pilancón E
	8.0	C-02-	77	685,310	2,097,608	2,971	Texmola N
	8.8	C-02-	87	688,732	2,098,854	2,858	S Chinela
	9.2	C-02-	13	689,327	2,098,937	2,742	Agua Escondida
	9.4	C-02-	2	689,822	2,098,937	2,682	Agua Escondida E
	9.9	C-02-	12	690,093	2,098,744	1,196	Xometla
	10.4	C-02-	65	690,714	2,098,971	2,610	Xometla
	11.8	C-02-	17	686,885	2,094,235	2,660	Loma Grande
	12.2	C-02-	11b	692,496	2,098,096	2,417	El Lindero N
	12.6	C-02-	11	692,587	2,097,922	2,379	El Lindero N
	13.1	C-02-	10	693,097	2,097,601	2,260	El Lindero S
	13.4	C-02-	18	689,766	2,093,572	2,550	San Isidro Berro
	14.4	C-02-	26	695,014	2,098,607	2,160	Cumbre del Español
	14.8	C-02-	27	633,266	2,099,575	2,180	Cumbre del Español
	15.4	C-02-	33	695,631	2,097,170	2,533	El Zapote
S	7.6	C-02-	108	681,594	2,097,417	3,302	N Texmalaquilla
	9.5	C-02-	20	680,840	2,095,627	3,200	Texmalaquilla
	9.6	C-02-	14	685,009	2,095,884	2,915	Texmola N
	10.0	C-02-	24	680,395	2,095,274	3,100	Texmalaquilla
	10.6	C-02-	19				
	11.0	C-02-	90	685,140	2,094,861	2,845	Texmola
	11.8	C-02-	16	686,401	2,093,543	2,690	Loma Grande
	12.3	C-02-	25	684,281	2,092,812	2,708	Paso Carretas
	14.8	C-02-	107	677,734	2,091,127	2,752	Texmalaquilla
	16.0	C-02-	1	676,918	2,090,266	2,680	Atzitzintla
	16.8	C-02-	15	688,292	2,089,056	2,240	Sierra de Agua
	24.0	C-02-	78	686,643	2,081,608	1,500	Maltrata
SW	5.1	C-02-	23	679,900	2,100,325	3,950	Sierra Negra
	5.2	C-02-	22	678,817	2,100,923	4,030	Sierra Negra
	5.3	C-02-	21	679,382	2,100,187	3,960	Sierra Negra
W	8.9	C-02-	104	674,139	2,108,385	3,097	Llano Grande
	9.5	C-02-	103	673,076	2,106,762	3,051	Llano Grande
	12.8	C-02-	105	670,239	2,108,944	2,871	S.M. El Aserradero
	14.0	C-02-	106	669,353	2,110,112	2,813	Ávalos
	18.5	C-02-	58	664,525	2,099,811	2,600	Cd. Serdán
NW	6.1	C-02-	82	679,598	2,110,022	3,908	E Miguel Hidalgo
	6.5	C-02-	81	679,400	2,110,459	3,842	E Miguel Hidalgo
	6.8	C-02-	80	678,684	2,110,702	3,840	E Miguel Hidalgo
	6.9	C-02-	61	677,659	2,110,039	3,400	Miguel Hidalgo
	7.1	C-02-	94	678,708	2,110,945	3,720	N Pico
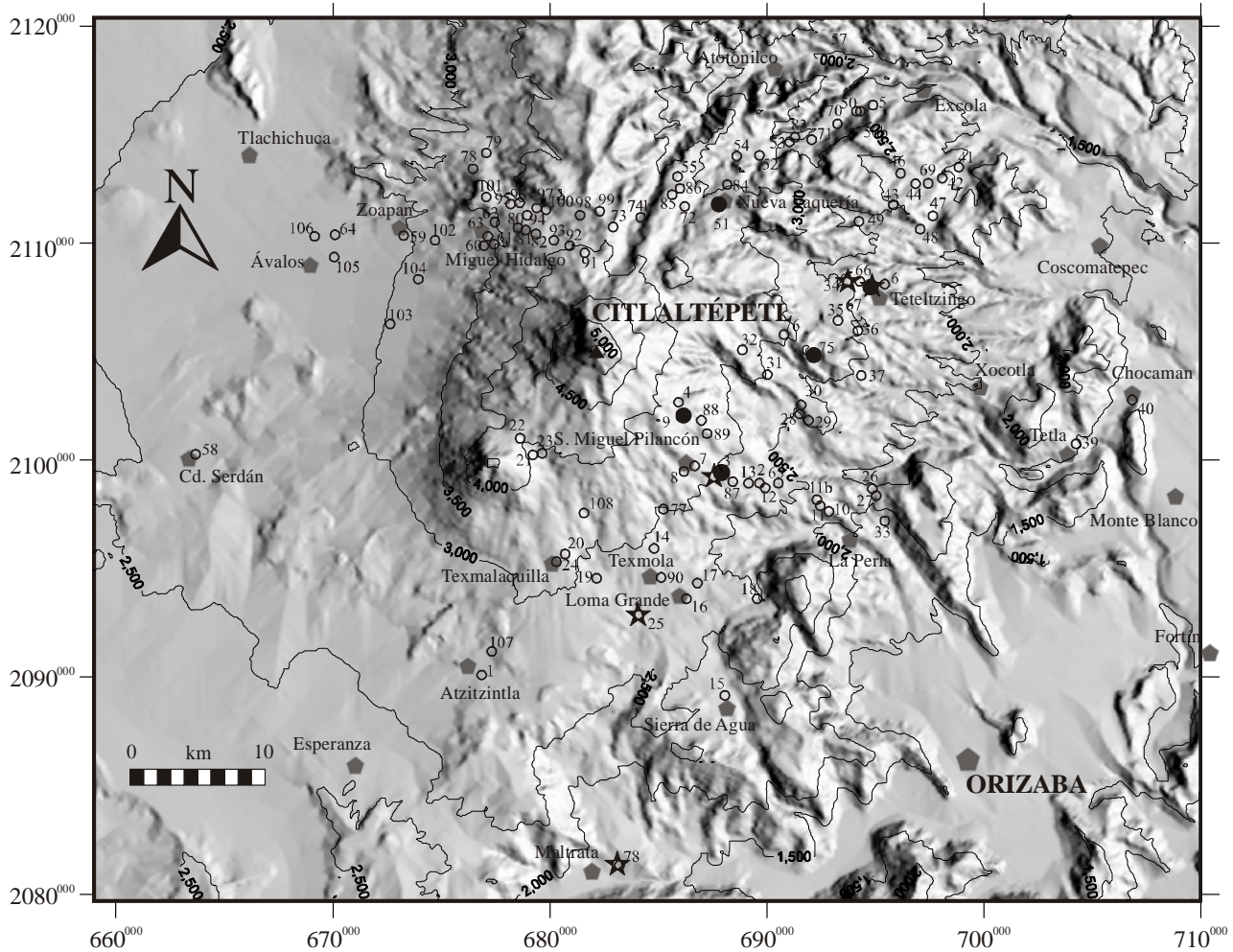
Figure 2. Location of sampling sites (open circles), log sections (bigger black dots) and villages (pentagons) around Citlaltépetl volcano. Digital Elevation Model from INEGI in UTM geographic units. Note that the numbers close to each circle refer to the last two digits of the correspondent section name in Table 1, shortened for graphic purposes (*e.g.*, 75 corresponds to C-02-75). Stars represent sections in Figure 4.

the different outcrops. The two end-members of such scale are a pile of loose dry sand (degree 1) and a high grade (rheomorphic) welded ignimbrite (degree 10). Intermediate degrees are determined in accordance to definitions shown in the scale.

STRATIGRAPHY AND COMPOSITION OF CITLALTÉPETL PUMICE DEPOSITS

The Citlaltépetl Pumice (CP) is a centimeter- to meter-thick sequence of lapilli and ash fallout layers interbedded whit thin ash layers and locally with pyroclastic flow deposits, which where formerly grouped as the Citlaltépetl Ignimbrite (Carrasco-Núñez and Rose, 1995). The CP sequence rests on a dark ash-sized meter-thick, partially humified deposit (layer Z), and crops out in several localities up to a distance of 24.6 km (C-02-40) from the vent, especially in the E and SE sectors of the volcano (site 40 in

Figure 2). The total thickness of the fall sequence decreases with distance: *e.g.*, from 112 cm at 6.5 km (C-02-8) to 2 cm at 24 km (C-02-78). In topographic heights, the pyroclastic sequence is dominated by fallout deposits (CP *sensu strictu*), but in topographic lows, several pyroclastic flow deposits belonging to the Citlaltépetl Ignimbrite are intercalated at different levels with the fallout deposits. At least four main pyroclastic flows were identified within the fallout sequence and they are numbered here from the oldest to the youngest. However, since the flow deposits were described elsewhere (Carrasco-Núñez and Rose, 1995), we are here focusing mainly on the fallout sequence.

The composite vertical section presented in this paper (Figure 3) represents the integration of different correlated sections and it does not belong to any specific site, even though in some locations (*e.g.*, C-02-3, C-02-75 and C-02-67) it is possible to recognize almost the entire sequence. The Citlaltépetl Pumice fallout sequence is formed by four main clast supported lapilli-sized beds (A, C, E+F, and H),

intercalated with four thin fine lapilli to coarse ash layers (A0, B, D, and G) as described below.

Layer Z

Layer consisting of a highly humified meter-thick gray-black ash deposit with abundant small charcoal fragments in the middle and upper position.

Layer A0

This layer is a ~3 cm thick, gray, crystal-rich, ash deposit with compaction degree 2. It sits in erosional contact with the humified black Z layer, and is composed entirely of highly broken crystals of pyroxene (65 vol.%), plagioclase (30 vol.%) derived from fragmented lithic clasts, shards of transparent juvenile glass and vitric scoria (4 vol.%), and pumice (1 vol.%). An apparent good sorting and some grading in the topmost part is observed. Layer A0 is always present at the base of the lowermost scoria flow and is more difficult to identify on topographic heights sections where it appears as a discontinuous layer, underlying layer A.

Scoria flow (1)

This metric-thick, massive and ungraded, black, scoria-rich deposit rests in direct contact on top of A0. Most juvenile clasts are large (over 30 cm in diameter), dense (with small vesicles), andesitic in composition with bread-crusted surfaces, and with thick intra-bubble walls. A diagnostic feature is the abundance of white dacitic inclusions in the juvenile material. The deposit contains a few rounded white pumice clasts and rare lithic clasts. Huge carbonized logs and branches are embedded and well preserved at the base of the deposit, with abundant sub-metric degassing pipe structures. The deposit is locally sealed by a lahar deposit (Figure 4) and by another similar scoria flow event in section C-02-25 (see Figure 2 for location).

Layer A

Defined as a pumice-rich (~66 vol.%), well-sorted, clast-supported, reverse- to normally-graded fallout layer containing gray and banded subangular pumice clasts with diagnostic white inclusions in them. In most sections, layer A shows reverse grading with upwards grain size variations from medium lapilli at the base to coarse lapilli in the center to fine lapilli at the top (normal grading). The most important feature of this layer is the presence of three different pumice types, which in order of abundance are: gray-yellow, black, and banded pumice. Table 3 shows the modal analysis for the pumice and scoria clasts.

The gray-yellow pumice contains submillimetric plagioclase (average 6.5 vol.%), pyroxene phenocrysts (average 6.2 vol.%), and only a few amphiboles phenocrysts (average 0.3 vol.%) (Table 3). The pumice shows thin bubble walls and elongated to fibrous vesicles. Black pumice clasts contain slightly less plagioclase (average 5.5 vol.%), lesser pyroxene (average 3.5 vol.%), but relatively abundant amphibole phenocrysts (average 10.1 vol.%) (Table 3), all within a glass matrix as all pumice clasts in the CP. Black pumice are the only clasts found in the whole sequence with such high abundance of amphibole crystals. Banded pumice is more scoriaceous when compared with light-color pumice, with often bigger and more rounded vesicles in the dark bands but with no variation in vesicularity between dark and light bands. The bulk deposit contains about 34 vol.% of angular gray andesitic lava clasts, in general smaller than the associated pumice. It shows a compaction degree of 1–3 and a bulk density of 620 kg/m³.

Mainly on the basis of the observed granulometric characteristics, layer A is subdivided in three parts: 1) the lower one, up to ~20 cm in thickness, is generally finer than the rest of the layer, with mean clast diameter of -1.96 Φ and mean sorting of 1.26. It is locally altered at its lower part due to the sharp, erosional contact on a thick gray ashy charcoal rich soil (layer Z). 2) The middle part, up to 15 cm in thickness, is generally the coarsest part of the entire layer (Md = -3.02 Φ) and shows a sorting of 1.55. 3) The topmost part has 5 to 10 cm of thickness, with a mean clast diameter of -2.52 Φ and a sorting of 1.63. Its

Table 2. Summary of granulometric and physical parameters for the components of each layer in the stratigraphic sequence shown in Figure 3. Mean diameter and sorting values have been averaged from 13 measurements. Pumice and lithic wt.% has been averaged from up to 25 samples. Key to the stratigraphic position within the deposit: low=lower part; mid=middle part; up=upper part of the layer. Please refer to text for details.

	Units	A0	A low	A mid	A up	B low	B up	C	D low	D up	E	F low	F up	G	H
Mean diameter (Md)	phi	-1.00	-1.96	-3.02	-2.52	-1.00	-1.30	-3.21	0.75	0.00	-1.91	-2.05	-1.05	0.54	-2.71
Mean sorting	Sigma	–	1.26	1.55	1.63	2.12	1.89	1.96	1.82	2.36	1.80	2.16	1.96	1.72	2.06
Bulk layer density	kg/m³	–	620	620	620	–	–	680	–	–	860	650	650	–	630
Juvenile clasts	wt. %	~60	66.37	66.37	66.37	81.94	–	66.45	59.77	–	44.26	70.91	61.91	70.72	64.36
Lithic + altered lava	wt. %	~40	33.63	33.63	33.63	18.06	–	33.55	40.23	–	55.74	29.09	38.09	29.28	35.64
Compaction	–	2	1–3	1–3	1–3	3	3	3–2	3	3	2	1–3	1–3	3	1–3

lower limit is markedly transitional, whereas its upper limit is sharp, mainly due to physical and granulometric differences with the lower part of layer B.

Layer B

Defined as a thin (2 to 5 cm) indured red-brown coarse ash (compaction degree 3) pumice-rich deposit, layer B contains an average of 82 vol.% of pumice and an average of 18 vol.% of lithics and a few coarse lapilli pumice clasts similar to those of the lower part of layer A. Both juvenile pumice and lithic clasts have a maximum diameter of 0.3 cm and they show poor angularity (pumice is much more rounded than lithic portion) and local strong alteration.

In some places it is possible to distinguish a lower and an upper part. We notice that the lower part is slightly more altered respect the upper one, with sorting of 2.12 and median diameter Md = -1.0 Φ, while the upper part shows a slightly better sorting (1.89) and a coarser clasts

size (Md = -1.3 Φ).

The limit between the upper and the lower part is not clear and the upper part is often missing. The upper contact is quite sharp due to strong compositional and granulometric differences with layer C.

Layer C

Consists of a centimetric (5 to 12 cm), white-pink, very coarse (Md = -3.21 Φ) lapilli pumice fallout deposit (66 vol.% of pumice and 34 vol.% of lithic clasts in average), often containing diagnostic white-pink pumice clasts, which can be larger that the average layer thickness. Layer C has a sorting of 1.96 and is slightly coarser in its middle part with compaction degree 2–3. In this layer, the pumice clasts show a relative abundance of total phenocrysts (33.2 vol.%) respect to the other layers. In particular, they contain 26.5 vol.% of plagioclase, 5.5 vol.% of pyroxene and only 0.7 vol.% of amphibole (Table 3). With respect to the pumice

Table 3. Modal analysis of 23 pumice thin sections. Point counted scanning of minimum of 500 points. *: dark pumice; Vd: vesicularity directly measured by optical scanning of the thin section. In italics the average values for each layer. Limit between microphenocrysts and phenocrysts is 2 mm.

Layer	Sample number	Px (vol. %)	Amph (vol. %)	Opaque (vol. %)	Plg (vol. %)	Tot. phenocr. (vol. %)	Matrix (% glass)	Tot (vol .%)	Vd (vol. %)
A	C-02-32a	6.3	0.2	0.0	3.0	9.6	90.4	100.0	42.40
A	C-02-51y	5.3	0.3	0.0	13.6	19.2	80.8	100.0	36.00
A	C-02-33b	7.1	0.3	0.2	2.8	10.4	89.6	100.0	49.00
Mean %		*6.2*	*0.3*	*0.1*	*6.5*	*13.1*	*86.9*	*100.0*	*42.50*
A*	C-02-2b	1.7	12.5	0.2	8.6	23.0	77.0	100.0	66.80
A*	C-02-30a	6.5	11.7	0.0	2.2	20.4	79.6	100.0	59.00
A*	C-02-3a (2)	4.2	7.6	0.0	5.6	17.4	82.6	100.0	33.00
A*	C-02-4a'	1.8	7.8	0.6	7.8	18.0	82.0	100.0	37.20
A*	C-02-3a (1)	3.1	11.1	0.0	3.4	17.6	82.4	100.0	24.00
Mean %		*3.5*	*10.1*	*0.2*	*5.5*	*19.3*	*80.7*	*100.0*	*44.00*
C	C-02-7c	4.7	0.1	0.0	25.8	30.6	69.4	100.0	33.40
C	C-02-3c	3.1	0.1	0.0	42.4	45.6	54.4	100.0	56.40
C	C-02-4c'	8.6	1.8	1.6	11.4	23.4	76.6	100.0	64.00
Mean %		*5.5*	*0.7*	*0.5*	*26.5*	*33.2*	*66.8*	*100.0*	*51.30*
E	C-02-6a	3.4	2.2	0.0	18.0	23.6	76.4	100.0	45.40
E	C-02-51a	5.2	1.4	0.0	14.6	21.2	78.8	100.0	30.60
E	C-02-34a	5.1	1.7	0.0	4.8	11.6	88.4	100.0	23.40
E	C-02-66c	8.8	2.8	0.0	8.8	20.4	79.6	100.0	46.00
Mean %		*5.6*	*2.0*	*0.0*	*11.6*	*19.2*	*80.8*	*100.0*	*36.40*
F	C-02-51b	5.4	0.0	0.0	14.2	19.6	80.4	100.0	46.40
F	C-02-29c	14.6	2.6	1.4	7.2	25.8	74.2	100.0	39.80
F	C-02-16a	7.4	1.4	1.2	6.6	16.6	83.4	100.0	33.20
F	C-02-2c	12.1	0.1	1.0	14.4	27.6	72.4	100.0	41.00
F	C-02-6b	12.0	0.0	1.2	14.0	27.2	72.8	100.0	21.60
Mean %		*10.3*	*0.8*	*1.0*	*11.3*	*23.4*	*76.6*	*100.0*	*36.40*
H	C-02-3h	13.6	0.0	1.8	13.2	28.6	71.4	100.0	23.20
H	C-02-51d	7.2	0.2	0.6	8.4	16.4	83.6	100.0	63.40
H	C-02-7h	10.4	0.2	2.8	9.6	23.0	77.0	100.0	42.20
Mean %		*10.4*	*0.1*	*1.7*	*10.4*	*22.7*	*77.3*	*100.0*	*42.90*

Table 4. Empirical compaction degree scale. This scale is proposed to estimate the compaction degree of each single pyroclastic deposit layer.

Degree	Definition	Description
1	Completely loose	Up to 10% of the particles do not fall if touched
2	Almost completely loose	Up to 20% of the particles do not fall if touched
3	A few particles stay together	Up to 30% of the particles do not fall if touched
4	Many partilces stay together	Up to 40% of the particles do not fall if touched
5	Half of the particles stay together	Up to 50% of the particles do not fall if touched
6	More than half of the particles stay together	Up to 60% of the particles do not fall if touched
7	Not completely welded tuff	With a few fiamme and no flow structures
8	Welded tuff	With fiamme and flow structures if ignimbrite
9	Very welded tuff	With fiamme and flow structures if ignimbrite
10	Perfectly welded (granite-like) tuff	Rheomorphic

clasts in other layers, layer C pumice clasts are often fractured and altered to pink in color, with an overall relatively high vesicularity (51.3 vol.%). Layer limits are sharp, mostly due to granulometric differences with adjacent layers. If layer B and layer D are present, the lower and upper limits are respectively sharp.

Layer D_{low}

This layer consists of a very thin (2–5 cm) black coarse ash (Md=0.75 Φ) pumice deposit. It is poorly sorted (1.82), ungraded and with incipient humification in its upper part. It is similar to the lower part of layer B and also includes some pumice clasts of layer C, but here the presence of some organic matter is evident.

Subrounded and altered pumice ash (average 60 vol.%) is basaltic-andesitic in composition and is mixed with altered and subangular lithics of andesitic composition (average 40 vol.%). Its upper limit is sharp only because of color changes from black to light gray.

Layer X

Layer composed by a gray, loose (compaction degree 1) thin (a few cm maximum), ash-sized, crystal rich, granular supported discontinuous horizon. It contains ~50 vol.% of altered and rounded pumice clasts, ~35 vol.% of rounded lithic clasts of andesitic composition, with strong red-pink (hydrothermal?) alteration, ~5 vol.% of green amphibole and plagioclase crystals, and some lithic clasts light in color. Layer X limits are sharp and easy to detect due to the grain size and clear color difference. This layer is not always present in the stratigraphic columns, but can be found either overlaying layer C or Di, and it is underlying layer Ds or pyroclastic flow 2 (Figure 4).

Lithic-rich flow (2)

In some localities in topographic lows, such as site 25 (Figure 2), a metric-thick, lithic-rich flow deposit rests on layer X in erosional contact. This deposit contains abundant gray to pink matrix and lithic clasts with predominantly andesitic composition. The presence of abundant carbonized logs imbedded in the lower part of this deposit and the pinkish oxidation color, lead us to suggest a minimum emplacement temperature of 300° C (Papale and Rosi, 1993).

Layer D_{up}

Layer composed by a thin (2–5 cm), gray, very fine lapilli (Md=0.0 Φ) deposit with bad sorting (2.36) and ungraded. The layer contains 65 vol.% of clasts and 35 vol.% of matrix. Among the clasts, we found 44 vol.% of pumice, 32 vol.% of plagioclase, 11 vol.% of lithic clasts, 10 vol.% of pyroxene crystals, and 3 vol.% of vitric shards. Clast components present a maximum diameter of 0.3 cm, show a clear subangular shape, and very low alteration degree. Layer D_{up} upper limit is quite sharp due to strong compositional and granulometric differences with layer E. Layer D_{up} commonly contains some large coarse lapilli pumice clasts.

Layer E

Although layer E and F are part of a continuous deposit, we separated them into two distinct layers on the basis of marked differences in components and granulometry. Layer E is a well-sorted, coarse lapilli-supported (Md = -1.91 Φ), lithic-rich, brick-red in color, pumice fall layer. It shows sorting of 1.80, with no or slightly reverse grading in the upper part due to the transition to the coarser layer F. In addition to its color and lithic-rich diagnostic features, it has a remarkable nearly constant thickness (~10 cm). For instance, the thickness is (ordered by increasing distance from vent) 10cm, 9cm, 10cm, 9cm and 9cm at the respective representative sections C-02-7 (6.8 km), C-02-3 (7.9 km), C-02-30 (9.8 km), C-02-75 (10.0 km) and C-02-67 (12.8 km). Layer E is characterized by high content of gray andesitic lithic clasts (average 56 vol.%), with typical Mn-coatings reddish oxidation, that in part show prismatic jointing. Due to those unique characteristics, this layer was used as a stratigraphic marker for the sequence. Scoriaceous pumice clasts present in the

layer show a relative poor vesicularity (36 vol.%) (Table 3) and low content of total crystals (19 vol.%) in comparison with pumice clasts in other layers. Mineral components includes 5.6 vol.% of pyroxene, 2.0 vol.% of amphibole and 11.6 vol.% of plagioclase (Table 3). The lower contact is sharp due to granulometric and compositional contrast with layer D_{up}, although in some locations (*e.g.*, C-02-75) layer E lower limit is in sharp contact with the lower pyroclastic flow described above. On the other hand, the upper limit is always gradual into layer F.

Layer F

This fallout layer is coarse, lapilli-supported, pumice-rich (average 71 vol.%), and reverse- to normal-graded. A regular, lateral and vertical thickness continuity is observerd in most of the outcrops studied. The layer thickness, in order of increasing distance from vent, is respectively 42cm, 37cm, 35cm, 35cm and >30cm thick at the representative sections C-02-7 (6.8 km), C-02-3 (7.9 km), C-02-30 (9.8 km), C-02-75 (10.0 km) and C-02-67 (12.8 km). In most
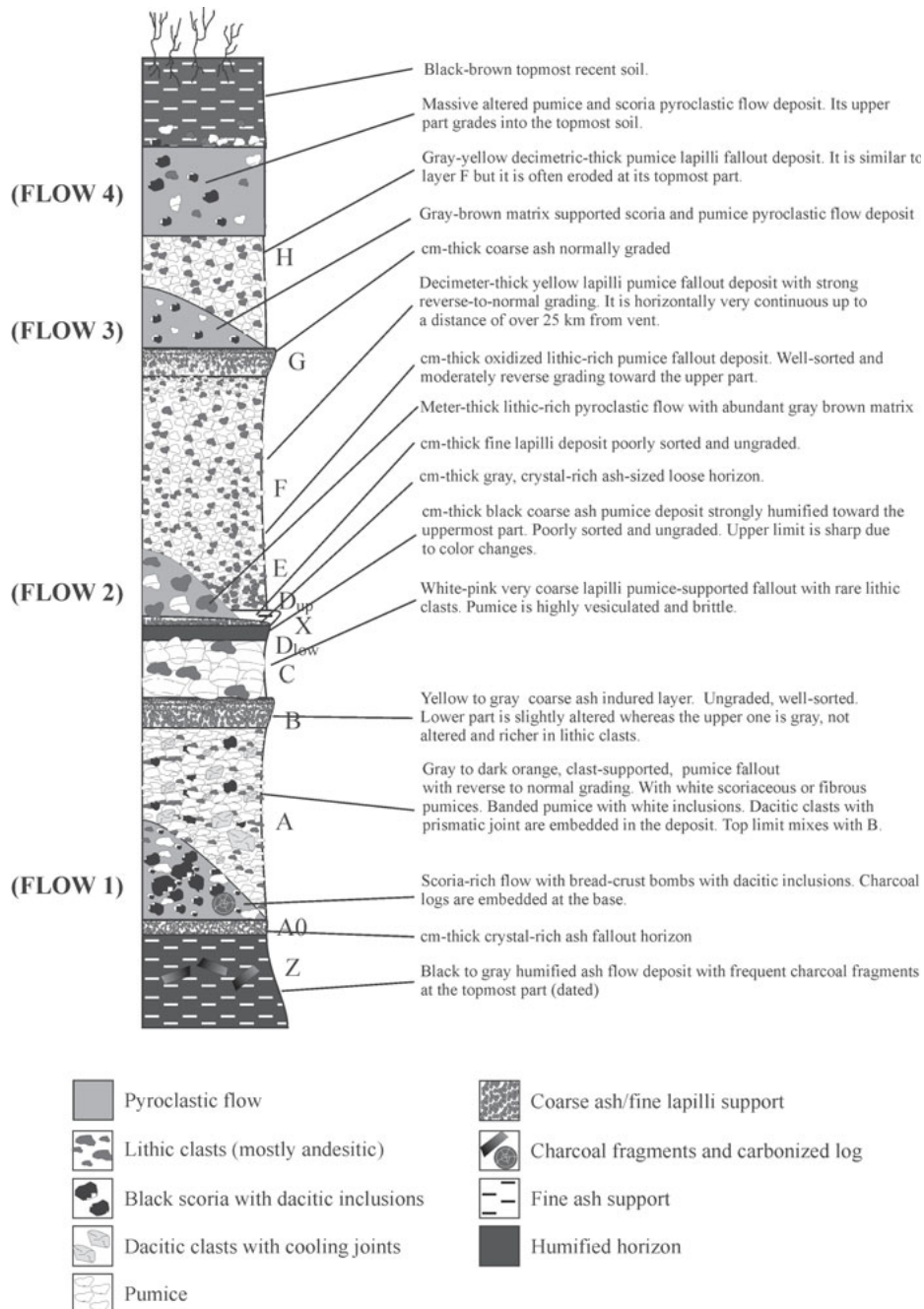
Figure 3. Composite section of the Citlaltépetl Pumice. Please refer to text for a detailed description of each layer.
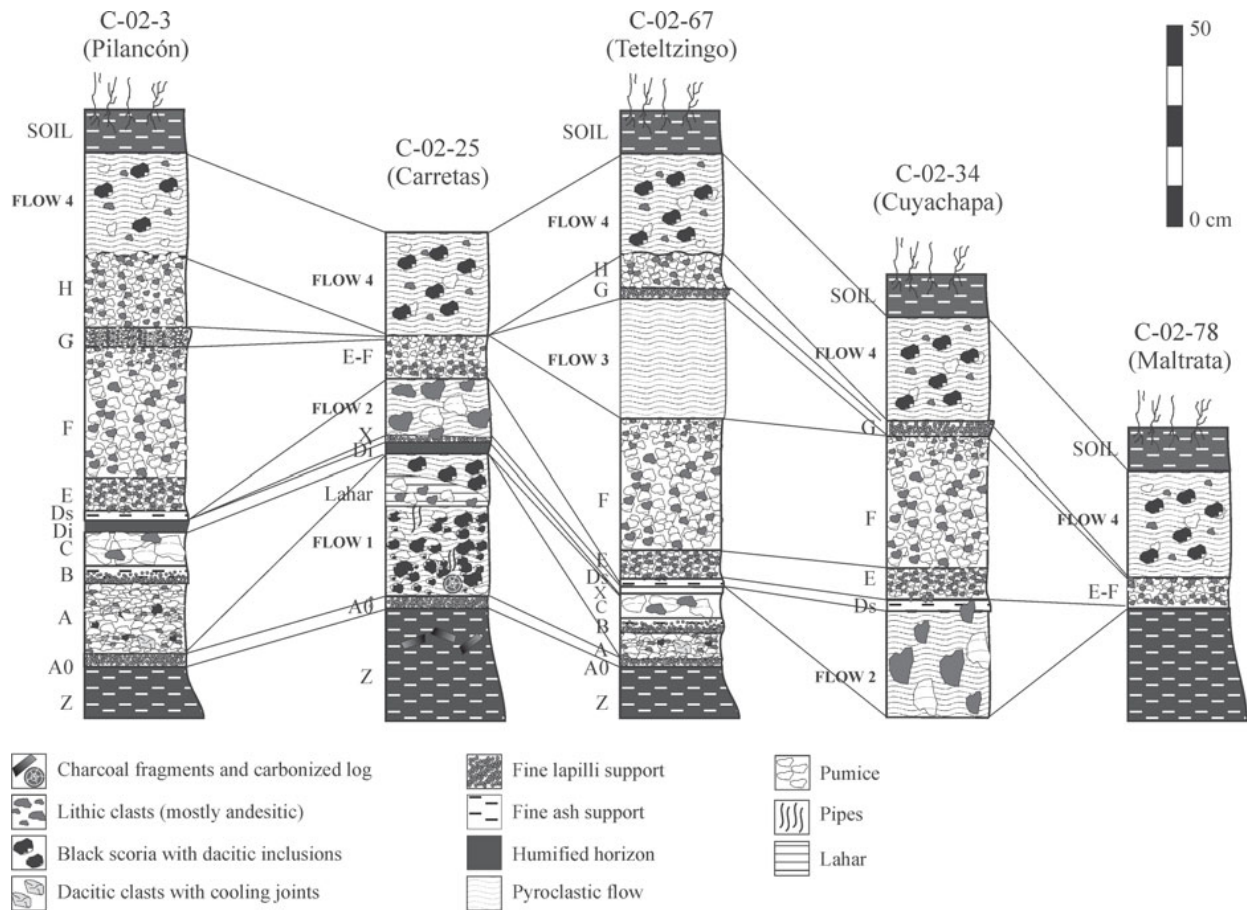
Figure 4. Correlation of key sections where the tephra fallout sequence (Citlaltépetl Pumice) and the pyroclastic flows (Citlaltépetl Ignimbrite) are related. See location of logs in Figure 2.

sections, layer F presents upward grain size variations from coarse lapilli at the base (Md = -2.05 Φ) to medium grain size at the top (Md = -1.05 Φ) , although the sorting remains quite constant through the section (2.16 at the lower part and 1.96 at the upper part). Layer F is very similar to layer A, but it does not show banded nor black pumice. The deposit contains on average 29 vol.% of angular gray andesitic lithic clasts, which in general are smaller than the pumice. Amphibole crystals are present only as traces (0.8 vol.%), plagioclase is abundant (11.3 vol.%), whereas pyroxene crystals abundance is higher than for other layers (10.3 vol.%). Pumice vesicularity is the same as in layer E pumice (36.4 vol.%) (Table 3). The lower boundary is transitional into layer E, which is part of the same deposit. The upper contact is sharp with layer G, however in some lower elevation locations such as in Teteltzingo area (*e.g.*, C-02-67) (see location in figure 2), layer F upper limit is in contact with the base of a centimetric-thick pyroclastic flow 3.

Layer G

This layer is thin, moderately-sorted (1.72), coarse-

ash (Md = 0.54 Φ), pumice-rich (~71 vol.%), and indurated, and contains lithic clasts of andesitic composition. It is characterized by being much more compacted (degree 3) and of finer grain-size than adjacent F and H layers; therefore its lower and upper limits are sharp and easy to recognize. Layer G thickness, in order of increasing distance from vent, is respectively 3cm, 6cm, 6cm, and 6cm, at the representative sections C-02-7 (6.8 km), C-02-3 (7.9 km), C-02-30 (9.8 km), C-02-75 (10.0 km) and C-02-67 (12.8 km). Layer G often shows coarser and more altered (humified) products in the lower part with respect to the upper one.

Pyroclastic flow (3)

In the canyon near Teteltzingo area (site 67 in Figure 2) a decimeter-thick pyroclastic flow deposit is found in erosional-sharp contact with the topmost part of layer F. The lower part is a 15 cm thick, gray-brown, matrix-supported horizon with a few pumice and lithic clasts. However, the thickness varies up to 2 meters in local topographic depressions. This deposit grades into the decimeters-

thick top part of the flow, which shows the presence of fine lapilli-sized pumice embayed in an abundant, gray-brown, ashy matrix. The lower part differs from top part mainly by the color and the relative increase in matrix alteration. This flow unit directly overlies layer F and underlies layer H in section C-02-67 (Figure 4 and 5).

Layer H

This layer consists of a gray to yellow, coarse lapilli-supported (Md = -2.71 Φ), pumice-rich (~64 vol.%), massive to stratified fallout deposit. The thickness is variable (5 to 20 cm), with bad sorting (2.06), and a fading normal
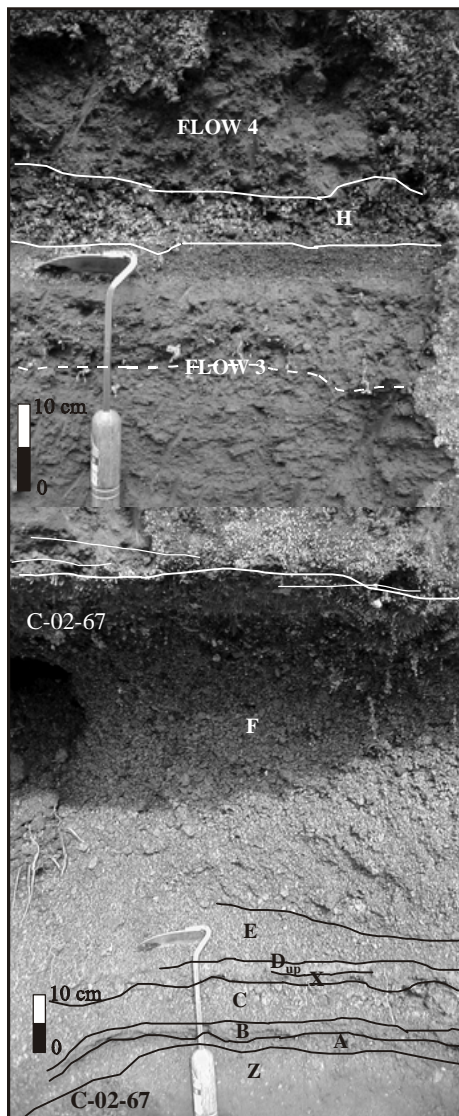
Figure 5. Photograph showing the fallout sequence of the Citlaltépetl Pumice and its relationship with the pyroclastic flows of the Citlaltépetl Ignimbrite (Carrasco Núñez and Rose, 1995) at the representative section C-02-67 nearby Tetetzingo village. See location 67 in Figure 2.

grading toward the topmost part. In order of increasing distance from vent, teh thickness is respectively 25cm, >18cm, >20cm, >15cm, and >5cm at the representative sections C-02-7 (6.8 km), C-02-3 (7.9 km), C-02-30 (9.8 km), C-02-75 (10.0 km) and C-02-67 (12.8 km). Because of its upper position, layer H topmost part is often eroded and therefore no reliable thickness measurement can be performed.

The deposit is similar to A and F in composition and clast-size characteristics: it is highly vesiculated (42.9 vol.%) or seldom fibrous and scoriaceous coarse pumice (64.4 vol.%) interbedded with lithic clasts (average 35.6 vol.%) of andesitic composition with a total content of microphenocrysts of 22.7 vol.% (10.4 vol.% of pyroxene, 10.4 vol.% of plagioclase, and only 0.1 vol.% of amphibole). The lower limit is sharp with layer G or with the middle flow in the Teteltzingo area, whereas the upper limit grades into a gray-brown upper pyroclastic flow deposit that corresponds to the upper member of the Citlaltépetl Ignimbrite (Carrasco-Núñez and Rose, 1995) described hereafter.

Pyroclastic flow (4)

In some localities (e.g. C-02-67 or C-02-35) (Figure 5) a decimetric to metric thick massive pyroclastic flow overlies layer H. This layer is a matrix-supported brown horizon with relatively abundant (~20%) altered and rounded pumice clasts up to 10 cm in diameter. It shows rare subrounded to subangular andesitic clasts with the same petrography as clasts in layer H. The lower part of the flow is in erosional contact with layer H, whereas the upper part grades into strong humified horizon and can often be confused with the weathered upper part of layer H whenever the flow is missing.

GRANULOMETRY AND COMPONENT ANALYSIS

The representative outcrop C-02-3 (site 3 in Figure 2) was selected for the discussion of the granulometric vertical variations and component analysis of each layer of the representative outcrop (Figure 6). Layer A shows a strong unimodal trend with relatively coarse modal diameter centered in -2 Φ and a marked positive skewness down to -7 Φ (fine tale). It is characterized by the relative abundant presence of dark scoriaceous pumice and scoria fragments, especially in the coarser fractions, in fact, no other layer contains this type of clasts. Layer B shows a wider gaussian curve with the mean diameter peak centered in 1 Φ and a notable fine tale, especially of 5 Φ. Dominant components are gray pumice and lesser abundant andesitic lithic clasts. Layer C shows a strong unimodal trend with coarse modal diameter (-1 Φ) and a modest positive skewness; this layer
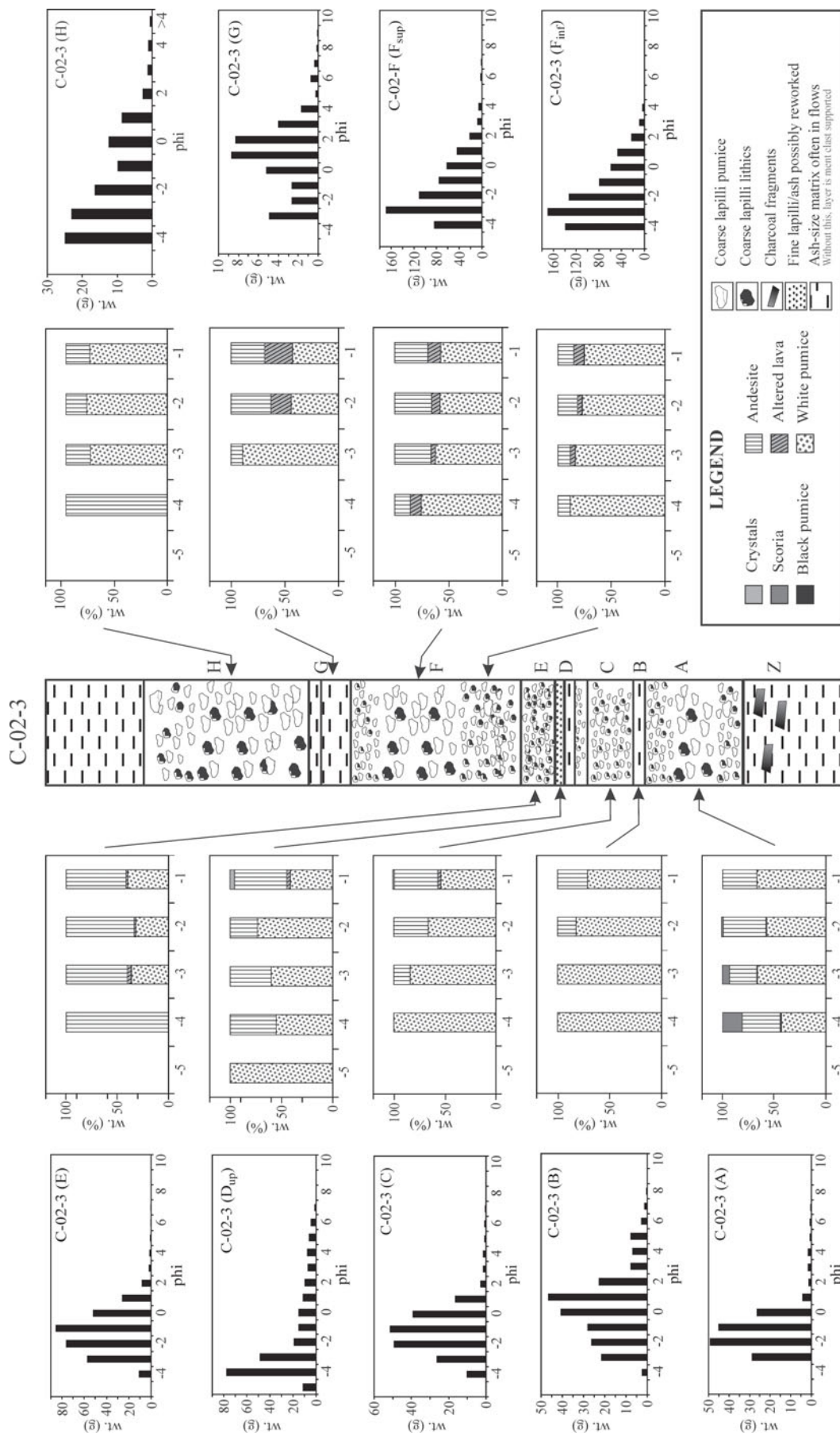
Figure 6. Grain-size distribution (outer plots) and component analysis (inner plots) for the most important layers at representative section C-02-3 (see site 3 in Figure 2). X axis=phi diameter; Y axis=weight (g) for the granulometry histograms and weight % for the component analysis histograms. Symbol size is proportional to grain-size plots values. F_{sup} and F_{inf} refer to the uppermost and lowermost part of layer F respectively. B and G samples were picked in the lower part of the respective layers, while A sample was picked in the middle part of layer A.

is composed of pink-gray pumice and andesitic lithics, more abundant in the finer fractions, and of a small amount of loose amphibole and plagioclase crystals in -1 Φ. Layer D_{up} shows a strong unimodal trend with modal main value centered in -4 Φ and a particularly characteristic positive skewness with abundant fine down to 9 Φ. Layer D_{up} main components are white pumice and andesitic clasts, especially in the coarser fractions, although in the finer fractions (-1 Φ) we found loose crystals of amphibole and plagioclase and some altered lithic clast. In layer E, the gaussian curve shows a strong unimodal pattern with high values of kurtosis (platokurtic), with the mean diameter centered in -1 Φ and almost lacking of fine fraction. As mentioned before, layer E shows the abundant presence of lithic clasts, especially in the coarser fraction, although some altered lava is also found in the finer fractions. Both, lower and upper parts of layer F (named F_{inf} and F_{sup} in Figure 6), as well as layer E, are strongly unimodal although slightly coarser with respect to layer E; the lower part (F_{inf}) shows a mean diameter value centered in -3.5 Φ, while the upper part (F_{sup}) has the peak centered in -3 Φ. Both parts, as well as layer E, show a modest positive skewness with a short fine tail generating high kurtosis values (platokurtic). Component analysis reveals for both parts of layer F a relatively abundant presence of altered lava along the constant presence of light pumice and andesitic lithic clasts. Layer G shows similar granulometric features as B and D_{up}: it shows some bimodality with a primary mean diameter peak centered in 1.5 Φ and a secondary peak centered in -3 Φ. Especially in the finer fractions, among the pumice fraction, we found abundant altered lava as well as andesitic clasts. Layer H displays a faded bimodal distribution with a main modal peak in -3.5 Φ and a small secondary one centered in 0 Φ. Its possible to notice a positive skewness, although we lack of data for the finer (>4 Φ) fraction. Component analysis shows a high percentage of lithic clasts in -4 Φ, whereas in the finer parts we notice the prevalence of gray-yellow pumice as in layers C and F.

As shown in Figure 6, altered lava clasts are not dominant, but they are more abundant in the uppermost layers, whereas rare scoria relicts were found only in a few sites of the lowermost layers (*e.g.*, layer A). Very rare crystals of amphibole, pyroxene and plagioclase, and glassy shards belonging to juvenile magma are found in the finer grain-size portions, especially in layers C and D.

Vertical variations in grain size parameters show in general an irregular behavior, however some general trends can be delineated (Figure 7). Note that for comparative purposes, samples from layers of finer granulometry such as B, D and G where connected separately from those samples representing the coarser deposit. For example, layer E shows a remarkable increase in the total lithic content with respect to the rest of the deposit; yet, this increase is not accompanied by an increase in the maximum size of lithic clasts. Moreover, the maximum size of pumice varies systematically in short cycles, with layers C, F and H

containing the largest pumice clasts in contrast to layers A and E (Figure 7c). The largest pumice clasts are present in layer F (Figure 7a), which is also the thickest fallout layer.

Usually, the vertical variation of median diameter shows a trend similar to the maximum pumice clast size. Vertical variations in sorting values are very irregular and do not show a defined trend. Andesitic accessory lithic clasts are the most abundant among the non-pumiceous population.

RADIOMETRIC DATING

In order to improve the data for stratigraphic correlation, five new charcoal samples were analyzed by means of conventional radiocarbon dating techniques (^{14}C) performed at the Radiocarbon Laboratory of Tucson University, Arizona by Professor Austin Long. The obtained results supplement the dates reported for the Citlaltépetl Ignimbrite by Carrasco-Núñez and Rose (1995), Siebe *et al.* (1993), and Heine (pers. comm., 1992) and are compared in stratigraphic sections in Figure 8. For other dates reported elsewhere (Höskuldsson and Robin, 1993) no geographic coordinates data are provided, and therefore were not included in this study (Table 5). The preexisting data for the lower pyroclastic flows of the Citlaltépetl Ignimbrite (PO 78, PO145, PO101B', PO133', PO101C and PO133) (Carrasco-Núñez and Rose, 1995) are in general in good agreement with dating we made from charcoal pieces collected in the layer Z at the base of the CP in sections C-02-4 (4z),C-02-8 (8z) and C-02-13 (13a). Carbon chunks picked up in the D and G fallout layers of sections C-02-8 (8d-d') and C-02-6 (6c), respectively, show dating results younger or at least comparable with the dating of the lower flows and older than the upper flows (PO101C and PO133), therefore in good agreement with field stratigraphy relationship. Sample 4z was collected at the bottom of the Z layer of the section C-02-4, 5 km SE of the main crater; this sample was dated at 9,475±160 yr. B.P. and is considered a bit older than other dates from the same stratigraphic level. Small charcoal pieces (13a) were collected 9.2 km from vent, in the middle part of Z layer and dated at 8,785±70 yr. B.P. In the section C-02-8 (near S. Miguel Pilancón) two samples were collected: one at the top of the Z layer (8z) and another one in the interface between D_{low} and D_{up} (8d–d'). The first sample yields a date of 8,640±50 years B.P., whereas the latter was dated in 8,825±155 years B.P. Dating of small charcoal fragments collected in correspondence with G layer of C-02-6 vertical section, 1 km NE of Teteltzingo village (6c), yields a value of 8,505±50 years B.P. Two further charcoal samples (C-02-2a and C-02-30z) were collected a few kilometers north from La Perla village and 10 km E of the Citlaltépetl crater, both within the upper layer Z. The first was dated 3,975±75 yr. B.P, whereas the second was dated 3,100±90 yr. BP. Both dates do not match with our expectations as
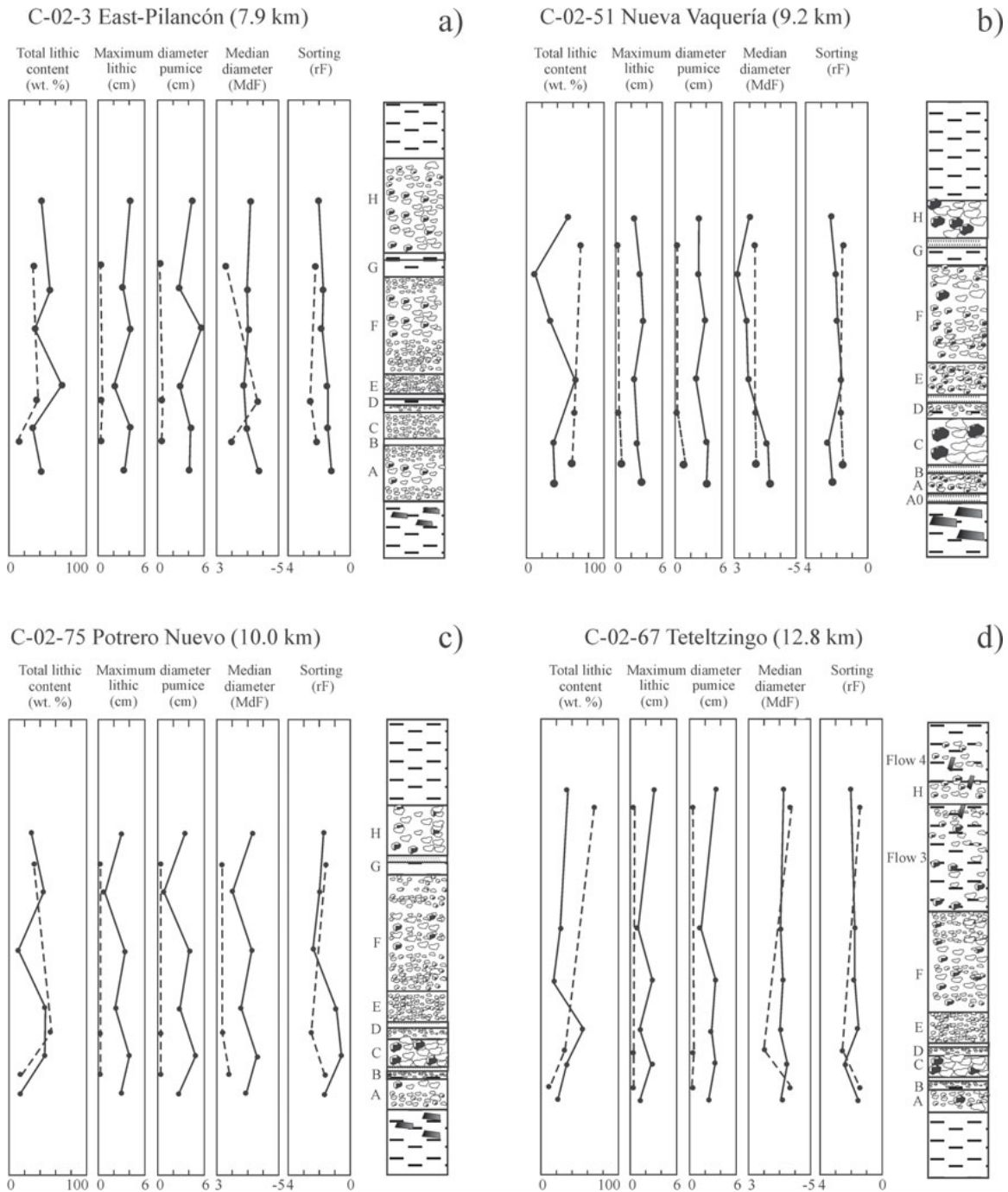
Figure 7. Lithic content, maximum size of pumice and lithic clasts, median diameter, and sorting values of four selected representative sections. Solid line: main pumice fallout deposit; dotted line: thin ash deposits. See Figure 2 for location.

they are much younger, therefore we assume that some sample contamination must have occurred, possibly through mixing with alien material.

Our radiocarbon dating, in conjunction with the previously mentioned data, supports the hypothesis that both the fallout sequence (CP) and the pyroclastic flow deposit (CI) are closely related in time within a period between 8.5–9.0 ka B.P.

STRATIGRAPHIC CORRELATION

Correlations between the Citlaltépetl Pumice fallout sequence with the Citlaltépetl Ignimbrite (Carrasco-Núñez and Rose, 1995) were facilitated by the identification of marker layers such as E, D_{low} and A0. In addition, in some localities pyroclastic flows interbedded with the CP sequence were also very useful to confirm stratigraphic
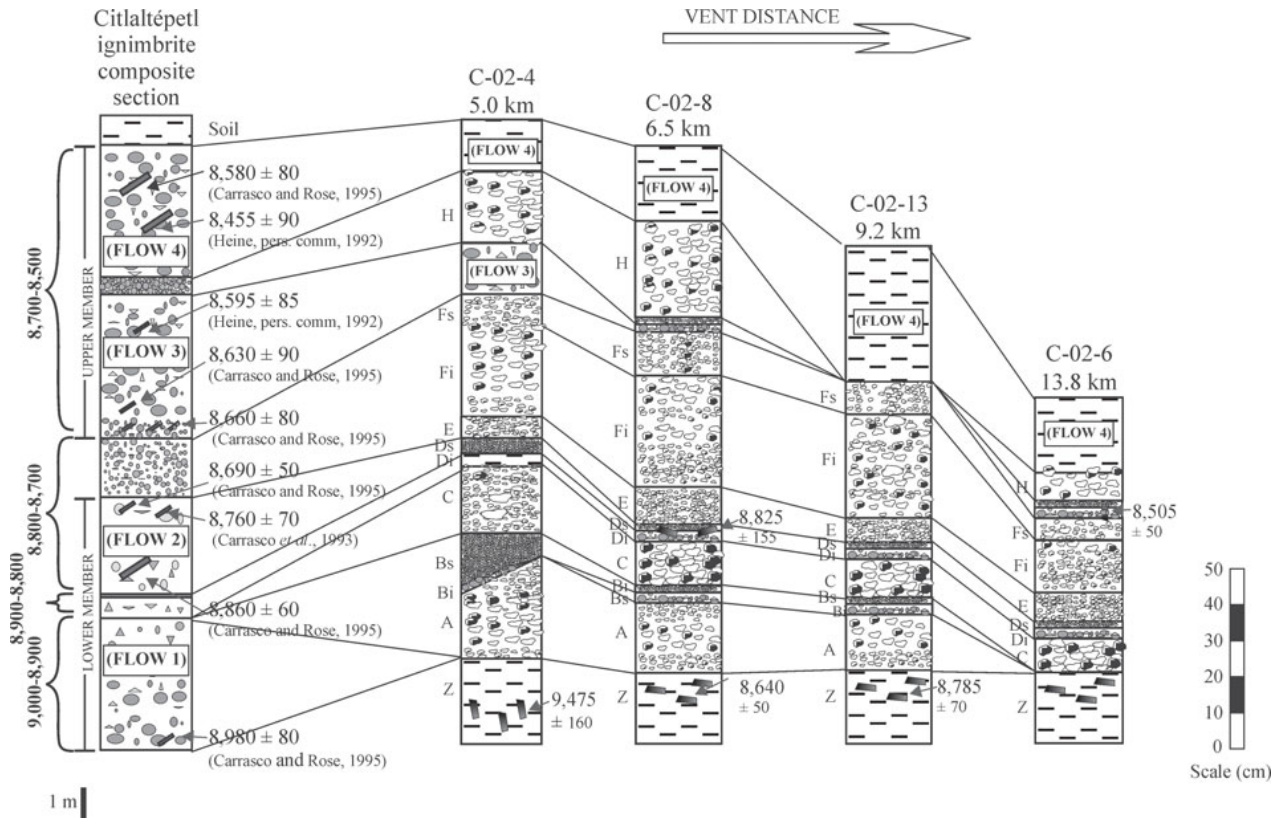
Figure 8. Correlation of log sections with radiocarbon data, compared with a composite column with ^{14}C data from Carrasco-Nuñez and Rose (1995) and Heine (1992, pers. comm). Ages are expressed in years B.P. Compare flow numbers with Figure 3. Dated deposits are grouped into 4 different eruptive episodes.

correlations (Figure 4). A more rigorous analysis of the reported radiocarbon dating and their respective errors, in conjunction with their relative stratigraphic position, suggests that the pyroclastic deposits are part of an eruptive epoch (*sensu* Fisher and Schmincke, 1984) that apparently includes at least four different eruptions or eruptive episodes, which can be separated in the following average ranges: 1) 8.9–9.0 ky B.P.; 2) 8.8–8.9 ka B.P.; 3) 8.7–8.8 ka; and 4) 8.5–8.7 ka B.P (Figure 9). Interpretation of layers B, D_{low}, and G as representing discrete time breaks, provide additional support to the correlations and radiometric dating to establish these episodes. Episode 1 represents the beginning of the eruptive epoch and groups the layer A0, the pumice fallout deposit A, and the lower part of the thin layer B (which can be correlated with a laharic and fluviatile unit reported by Carrasco-Núñez and Rose (1995) in the lower member of the CI) (Figure 9). After a short eruptive pause, represented by the upper part of layer B, the episode 2 is represented by the deposition of the pumiceous layer C and D_{low}, followed by the second repose in which D_{low} humifies. Episodes 3 is represented by the deposition of layer X, D_{up} and the pumice fallout deposit E+F, which was also used by Carrasco-Núñez and Rose (1995) to separate the upper from the lower units of the CI sequence. The episode 3 ends with the deposition of layer G, where its

incipient humification represents the third eruptive pause. Episode 4 is represented by the deposition of the topmost fallout layer H.

INTERPRETATION AND CONCLUSIONS

The whole sequence that forms the plinian Citlaltépetl Pumice deposit can be compared in style to the Holocene plinian eruptions of Popocatépetl (Siebe *et al.*, 1996) and the late Pleistocene plinian eruption of the Nevado de Toluca volcano (Arce *et al.*, 2003). CP was stratigrafically divided into four distinct lapilli pumice fallout deposits that represent four distinct eruptive episodes separated by three short eruption pauses (Figure 9). The millimetric lowermost ash-sized gray layer (A0), resting above the sharp discontinuity cutting the gray, humified ash deposit (layer Z), is interpreted as the result of the first explosive pulse that unclogged the preexisting conduit, similar to the first pulse of the Holocene plinian eruption of La Virgen volcano (Capra *et al.*, 1997). This was immediately followed by the emplacement of a dense scoria flow which destroyed the preexisting forest and incorporated many large carbonized logs, and then by the emplacement of the thick pumice fall deposit A. The characteristics of such deposit suggest a first

Table 5. Radiocarbon dating of recent Citlaltépetl deposits compared with preexisting dates by Carrasco and Rose (1995) and Heine (1992, pers. comm.). Data are either in degrees or in UTM units (quadrant 14 Q). *: Citlaltépetl Ignimbrite; R: Radiometric; AMS: Accelerator Mass Spectrometry.

Sample	^{14}C-Dates	Method	Deposit	Location	Place in layer	Long	Lat	Reference
Heine 1	8,544±90	R	Pyroclastic flow	–	–	–	–	Heine (pers. comm 1992)
Heine 2	8,595±85	R	Pyroclastic flow	–	–	–	–	Heine (pers. comm 1992)
PO-133	8,630±90	R	Scoria and pumice flow	Teteltzingo	Lower*	97º09.0'	19º09.5'	Carrasco and Rose (1995)
PO-101C	8,660±80	R	Scoria and pumice flow	Loma Grande	Lower*	97º14.9'	18º55.2'	Carrasco and Rose (1995)
6c	8,505±50	AMS	Fallout	Teteltzingo	Vertical in G	695,553	2,108,242	This work
8 d-d'	8,825+155/-150	R	Fallout	Pilancon W	Interface d-d'	686,214	2,099,672	This work
8z	8,640±50	AMS	Fallout	S. Miguel Pilancon	Top Z	686,214	2,099,672	This work
PO-133'	8,690±50	R	Scoria and pumice flow	Teteltzingo	Lower*	97º08.8'	19º03.3'	Carrasco and Rose (1995)
PO-101B'	8,760±70	R	Scoria and pumice flow	Loma Grande	Lower*	97º14.9'	18º55.2'	Carrasco and Rose (1995)
13a	8,785±70	R	Fallout	Agua escondida	Top Z	689,300	2,099,153	This work
PO-145	8,860±60	R	Scoria and pumice flow	Excola	Lower*	97º08.2'	19º08.1'	Carrasco and Rose (1995)
PO-78	8,980±80	R	Scoria and pumice flow	Maltrata	Lower*	97º13.8'	18º48.8'	Carrasco and Rose (1995)
4z	9,475±160	R	Fallout	S. Miguel Chinela (N)	Top Z	686,664	2,102,381	This work

eruptive column whose altitude varied with time.

After a short eruptive pause, a second eruptive column originated layer C. Although layer C is thinner than layer A, its pumice clasts are larger and indicate a relatively higher eruptive energy. The eruption gradually wanes as shown by the deposition of the thin ash layer D_{low} that marks the end of the second eruptive episode. The high grade of humification of layer D_{low} indicates a repose occurred before the beginning of the third eruptive episode.

The deposition of layer X and layer D_{up} witnesses the
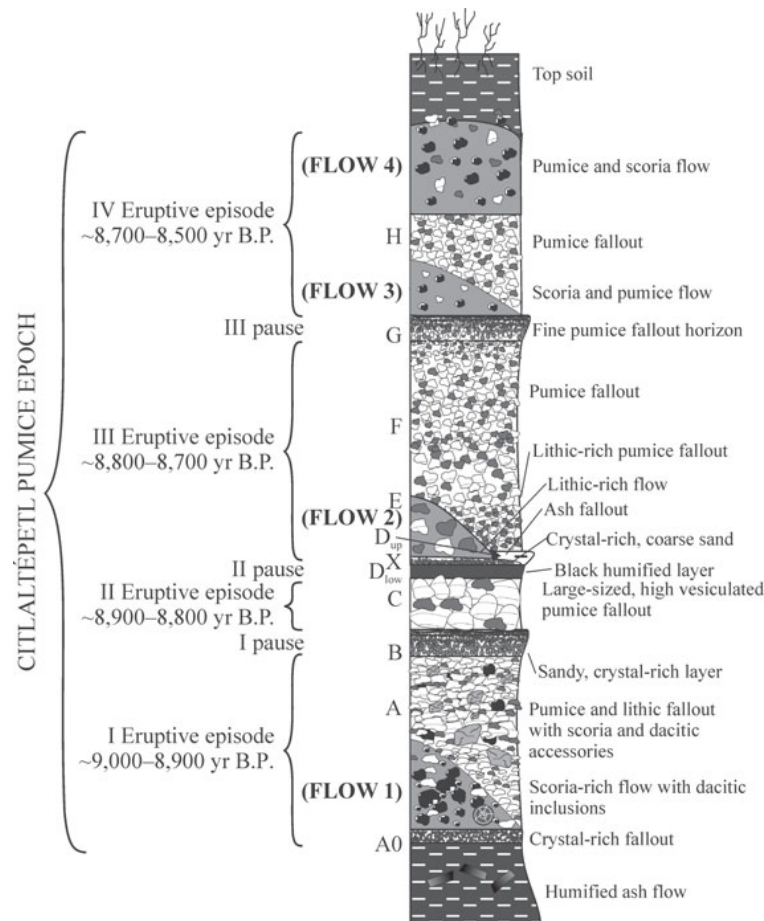
Figure 9. Interpretation of the Citlaltépetl Pumice stratigraphic sequence, which include four diferent eruptive episodes. Terminology is in accordance with Fisher and Schmincke (1984). Same legend as Figure 3. See text for details.

starting over of the activity that continues with the explosive activity represented by layer E+F (third episode). The sharp transition from the layer D_{up} to the coarser layer E was interpreted as a sudden waxing of the activity. The abundant presence of accessory lithics and the very good sorting of the layer E suggest that a maintained column eroded and widened the inner conduit diameter. Layer E gradually changes into the coarser and thicker pumice fall layer F, where the largest pumice clasts of the sequence are found. In spite of the grain-size divisions, layer E and layer F were interpreted as the product of a single continuous eruption. The inversely graded lower part of layer F suggests a growth of the paroxistic event due to the production of abundant vesiculated magma and wanes in accordance with the deposition of the topmost part of the layer F that shows a gradual decreasing in clasts diameter toward the top. The products of this third episode are sealed off by the thin and vanishing layer G, which is interpreted, as layer D_{low}, as a short eruption pause, as it also correlates with pyroclastic flow deposits in lower elevation sections.

A renewed plinian column is represented by the deposition of layer H. Overlying pyroclastic flows are apparently not related to the collapse of the column associated to layer H and apparently represent independent explosive activity as the components for each deposit are different.

These findings must be considered fundamental for the understanding of the eruptive process and are indispensable tools for the building of an eruption model, which will be the focus of a separated publication.

ACKNOWLEDGMENTS

REFERENCES

Arce, J.L., Macías, J.L., Vázquez-Selem, L., 2003, The 10.5ka Plinian eruption of Nevado de Toluca volcano, Mexico: Stratigraphy and hazard implications: Geological Society of America Bulletin, 115 (2), 230–248.

Capra, L., Macías, J.L., Espindola, J.M., Siebe, C., 1997, Holocene plinian eruption of La Virgen volcano, Baja California, Mexico: Journal of Volcanology and Geothermal Research, 80, 239–266.

Carrasco-Núñez, G., 1993, Structure, eruptive history and some major hazardous events of Citlaltépetl volcano (Pico de Orizaba), Mexico: Michigan, USA, Michigan Technological University, Ph.D. dissertation, 182 p.

Carrasco-Núñez, G., 1997, Lava flow growth inferred from morphometric parameters: a case study of Citlaltépetl volcano, Mexico: Geological Magazine, 134, 2, 151–162.

Carrasco-Núñez, G., 2000, Structure and proximal stratigraphy of Citlaltépetl volcano (Pico de Orizaba), Mexico: Geological Society of America, Special Paper, 334, 247–262.

Carrasco-Núñez, G., Rose, W.I., 1995, Eruption of a major Holocene pyroclastic flow at Citlaltépetl volcano (Pico de Orizaba), Mexico, 8.5–9.0 Ka: Journal of Volcanology and Geothermal Research, 69, 197–215.

Carrasco-Núñez, G., Vallance, J.W., Rose, W.I., 1993, A voluminous avalanche-induced lahar from Citlaltépetl volcano, Mexico: Implications for hazard assessment: Journal of Volcanology and Geothermal Research, 59, 35–46.

Crausaz, W., 1994, Pico de Orizaba or Citlaltépetl: Geology Archaeology, History, Natural History and Mountaineering Routes: Ohio, USA, Geopress International, 594 p.

Fisher, R.V, Schmincke, H.U, 1984, Pyroclastic Rocks: New York, Springer Verlag, 472 p.

Höskuldsson, A., 1993, Le complexe volcanique Pico de Orizaba-Sierra Negra-Cerro Las Cumbres (Sud-Est Mexicain): Structure, Dynamismes eruptifs et evaluacion des aléas: France, Clermont-Ferrand, Université Blaise Pascal, thèse de doctorat, 210 p.

Höskuldsson, A., Robin, C., 1993, Late Pleistocene to Holocene eruptive activity of Pico de Orizaba, Eastern Mexico: Bulletin of Volcanology, 55, 571–587.

Inman, D.L., 1952, Measures for describing the size distribution of sediments: Journal of Sedimentary Petrology, 22, 125–145.

Papale, P., Rosi M., 1993, A case of no-wind plinian fallout at Pululanga Caldera (Ecuador): implications for model of clast dispersal: Bulletin of Volcanology, 55, 523–535.

Robin, C., Cantagrel, J.M., 1982, Le Pico de Orizaba (Mexique): Structure et evolution d'un grand volcán andesitique complexe: Bulletin of Volcanology, 45 (4), 299–315.

Rodríguez, S.R., Siebe, C., Komorowski, J.C., Abrams, M., 2002, The Quetzalapa Pumice: A voluminous late Pleistocene rhyolite deposit in eastern Trans-Mexican Volcanic Belt: Journal of Volcanology and Geothermal Research, 113, 177–212.

Siebe, C., Abrams, M., Sheridan, M.F., 1993, Major Holocene block-and-ash fan at the western slope of ice-capped Pico de Orizaba volcano, Mexico: Implications for future hazards: Journal of Volcanology and Geothermal Research, 59, 1–33.

Siebe, C., Abrams, M., Macías, J.L., Obenholzner, J., 1996, Repeated volcan disasters in Prehispanic time at Popocatépetl, Central México: Past key to the future?: Geology, 24(5), 399–402.

Wohletz, K.H, 1983, Mechanism of hydrovolcanic pyroclastic formation: grain-size, scanning electron microscopy and experimental studies: Journal of Volcanology and Geothermal Research 17, 31–63.